

2016+112: A Gravitationally Lensed Type–II Quasar

L.V.E. Koopmans¹, M.A. Garrett², R.D. Blandford¹, C.R. Lawrence³,
A.R. Patnaik⁴ & R.W. Porcas⁴

¹*California Institute of Technology, mailcode 130-33, Pasadena CA 91125, USA*

²*Joint Institute for VLBI in Europe, P.O.Box 2, NL-7990 AA, Dwingeloo, The Netherlands*

³*Jet Propulsion Laboratory, California Institute of Technology, 4800 Oak Grove Drive, Pasadena, CA 91109, USA*

⁴*Max-Planck-Institut für Radioastronomie, Auf dem Hügel 69, D-53121 Bonn, Germany*

Accepted ... Received ...

ABSTRACT

A single-screen model of the gravitational lens system 2016+112 is proposed, that explains recent *Hubble Space Telescope* (HST) infrared (NICMOS–F160W) observations and new high-resolution *European VLBI Network* (EVN) 5–GHz radio observations, presented in this paper. In particular, we find that a massive ‘dark’ structure at the lens position, previously suggested by X-ray, optical and spectroscopic observations of the field around 2016+112, is not necessarily required to accommodate the strong lensing constraints. A massive structure to the north-west of the lens system, suggested from a weak-lensing analysis of the field, is included in the model. The lensed source is an X-ray bright active galaxy at $z=3.273$ with a central bright optical continuum core and strong narrow emission lines, suggestive of a type–II quasar. The EVN 5–GHz radio maps show a radio-jet structure with at least two compact subcomponents. We propose that the diamond caustic crosses the *counter-jet* of the radio source, whereas the steeper spectrum jet is only doubly imaged. This implies that different parts of the extended radio structure, narrow-line region and host galaxy are either doubly or quadruply imaged. Our lens model predicts a very high magnification ($\mu\sim 300$) of the inner two radio components of complex C. If the jet exhibits relativistic velocities on micro-arcsecond scales, it might result in apparent *hyperluminal* motion. However, the lack of strong radio variability, the peaked radio spectrum and the inference that it is the counter-jet that crosses the caustic do not support this notion at present. Superluminal motion might be more likely. Our model furthermore implies that the optical spectrum of image C’ will only show features at the same redshift as the AGN.

Key words: Gravitational lensing – quasars: general – radio continuum: general

1 INTRODUCTION

The gravitational lens system 2016+112, discovered by Lawrence et al. (1984), has defied any simple explanation. The system consists of two AGN images (A and B) at a redshift of $z=3.273$ (Lawrence et al. 1984; Schneider et al. 1985, 1986), separated by 3.4 arcsec. Early optical and near-infrared observations (e.g. Schneider et al. 1985; Langston, Fischer & Aspin 1991; Lawrence, Neugebauer & Matthews 1993) showed the presence of two extended objects (designated C’* and D). C’ lies some 2 arcsec south-east of image B, such that ABC’ nearly form a right triangle. Image D, the primary lens galaxy, has a redshift of 1.01 (Schneider et al.

1985) and is close to the centroid of the images A, B and C’. The redshift of C’ has resisted measurement. Narrow Ly- α emission near A, B and C’ has been detected at a redshift of $z=3.273$ with line widths $\lesssim 1000 \text{ km s}^{-1}$ (Schneider et al. 1986, 1987; Lawrence 1996; Yamada et al. 2001; Lawrence et al. 2001). Similarly, two fuzzy patches of Ly- α emission were detected about 3 arcsec north-west and west of images A and B, respectively (Schneider et al. 1986, 1987). Recent deep high-resolution optical and IR observations with the HST in *I*-band (Lawrence et al. 2001) and F160W-band (NICMOS) (see the CASTLES webpage <http://cfa-www.harvard.edu/glensdata/MG2016.html>; e.g. Muñoz et al. 1998), respectively, show that images A and B are unresolved and compact, whereas image C’ is arc-like and does not show obvious compact structure.

At radio wavelengths, 2016+112 has been observed with the VLA (e.g. Lawrence et al. 1984; Schneider et al. 1985).

* The prime distinguishes it from the radio structure (designated C), which early on was not known or thought to be associated with the optical emission.

All components contain compact substructure in higher resolution MERLIN (Garrett et al. 1994), VLBI (Hefflin et al. 1991) and EVN (Garrett et al. 1996) images. Whereas components A and B consist of at least two subcomponents (oriented approximately north-west), radio component C splits in four dominant subcomponents aligned east-west (e.g. Garrett et al. 1996). Components A and B have steep integrated radio spectra between 18 and 6 cm (Lawrence et al. 1994), whereas component C has a somewhat flatter integrated radio spectrum. All component spectra steepen between 6 and 2 cm (Langston et al. 1989). The overall integrated spectrum of the lens system is that of a GPS source and peaks somewhere in the range of 1 to 5 GHz. With the VLA in A-array, the source is barely detectable at 22 GHz (Patnaik, private communication). In addition, EVN observations at 18 and 6 cm (Garrett et al. 1996) show that the two outermost images (C_{11} and C_2) have a significantly steeper spectrum than the two innermost components (C_{12} and C_{13}). These observations suggest that the structures $C_{11}+C_{12}$ and $C_{13}+C_2$ have opposite parities and are probably images of the same structure in the source.

Observations of the field around 2016+112 with the *ASCA satellite X-ray Observatory* suggested the presence of diffuse X-ray emission centered on the lens system and to the north-west (Hattori et al. 1997; Benitez et al. 1999). Recent observations with the *Chandra X-ray Observatory*, however, unambiguously show that this emission is entirely due to discrete sources and not diffuse cluster emission (Chartas et al. 2001). In addition, the lensed images are detected. The presence of X-ray and narrow emission lines suggests that the source could in fact be a type-II quasar (e.g. Yamada et al. 2001; Chartas et al. 2001). None of the other X-ray sources in the field are associated with galaxies detected by Soucail et al. (2001; see below). The comparatively large number of X-ray sources in the field of 2016+112 might be the result of a magnification bias, which enhances the number count of sources around the lensing mass distribution if the number density of X-ray source increases steeply at redshifts larger than that of the lens galaxy.

Spectroscopic observations by Soucail et al. (2001) show the presence of an overdensity of galaxies at the same redshift as lens galaxy D. Similarly, Clowe et al. (2001) detect a $3\text{-}\sigma$ weak-lensing signal to the north-west of the lens system, roughly coincident with the region of excess X-ray emission (e.g. Benitez et al. 1999). The latter could again be due to a magnification bias. Only a marginal weak-lensing signal at the position of the lens system was found, consistent with the absence of a very massive dark X-ray cluster.

Several models have been proposed to explain these observations. Some employ single deflector and single-screen models (Langston et al. 1991; Benitez et al. 1999), whereas others have used more complex models with C' and D being different galaxies (Narashima et al. 1987). In the proposed two-screen models it is assumed that object C' is a galaxy at a redshift different from galaxy D, and responsible for lensing radio complex C in additional ‘subimages’ (Nair 1993; Nair & Garrett 1997). The suggestion of mirror-symmetry and opposite parities for the structures $C_{11}+C_{12}$ and $C_{13}+C_2$ would probably favour a single-screen model over most two-screen models, based on Ocam’s razor, as it no longer requires a second conveniently placed lens to explain the observed image structure. However, a two-screen

model or a model that has two lens galaxies in the same lens plane, predicting the same parities as a single-screen single-lens model (Nair & Garrett 1997) can ofcourse not be excluded based on this argument alone.

In this paper we propose an alternative model that can quantitatively explain these observations with a single screen. Instead of explaining the lens system with a complex deflector model, we find it can also be explained by a realistic, although more complex source model. In Sect.2, we present EVN 5-GHz radio observations of 2016+112, which suggests that complex C consists of two images with opposite parities. In Sect.3, a detailed structure of the source is proposed which qualitatively can explain most of the observed features of the 2016+112 lens system. In Sect.4, we present a model of the lens potential that incorporates mass structures from the field around the lens system. In Sect.5, we compare the model to the observational constraints to find that it can also quantitatively explain the available observational constraints of the lens system and the field. In Sect.6, our results are summarized and discussed. Throughout this paper we assume a flat smooth Friedman-Robertson-Walker (FRW) universe with $\Omega_m=0.3$ and $H_0=65 \text{ km s}^{-1} \text{ Mpc}^{-1}$.

2 EVN 5-GHZ OBSERVATIONS AND DATA ANALYSIS

The 5-GHz EVN observations were made on 17–18 May 1995 from UT 22h30 to 10h30, using 7 antennas of the EVN: the 100-m Effelsberg (DE), 26-m Jodrell-Mk2 (UK), 25-m Onsala (SE), 32-m Medicina (IT), 32-m Noto (IT), 32-m Cambridge (UK), and Westerbork-array (NL). Technical problems resulted in no data from the latter two antennas. The recording mode was MkIIIa Mode A (56 MHz bandwidth, Left Hand Circular polarisation). A phase-reference observing scheme was used, switching between the target, 2016+112, and a compact calibrator, J2029+121, located 1 degree away. The tape ran continuously through each 13 minute pass, and the source switching cycle consisted of alternating between 90 seconds on the calibrator and 140 seconds on the target. Correlation of the data was conducted at the MPIfR MkIIIa correlator in Bonn. To prevent loss of data during correlator synchronisation of the very short scans, each baseline was correlated twice as a continuous tape pass, once at each of the two source positions. (Spurious correlations on the “wrong” source were edited out in the later data analysis).

Subsequent data processing and analysis was performed with the NRAO AIPS package. Long fringe-fitting solutions were made that included several switching phases of the calibrator; the resulting phase, delay and rate solutions were then applied to 2016+112. Although the interferometer model used in the MPIfR correlator was not sufficiently accurate to permit direct phase-referencing, this process did remove short-term phase fluctuations, and allowed longer solution intervals to be used for self-calibration of the phases of the 2016+112 visibilities. Amplitude calibration was made by initially assuming that J2029+121 is a 0.91-Jy point source on all baselines, and then determining self-calibration corrections after mapping the source. These amplitude and phase corrections were also applied to 2016+112. In order to

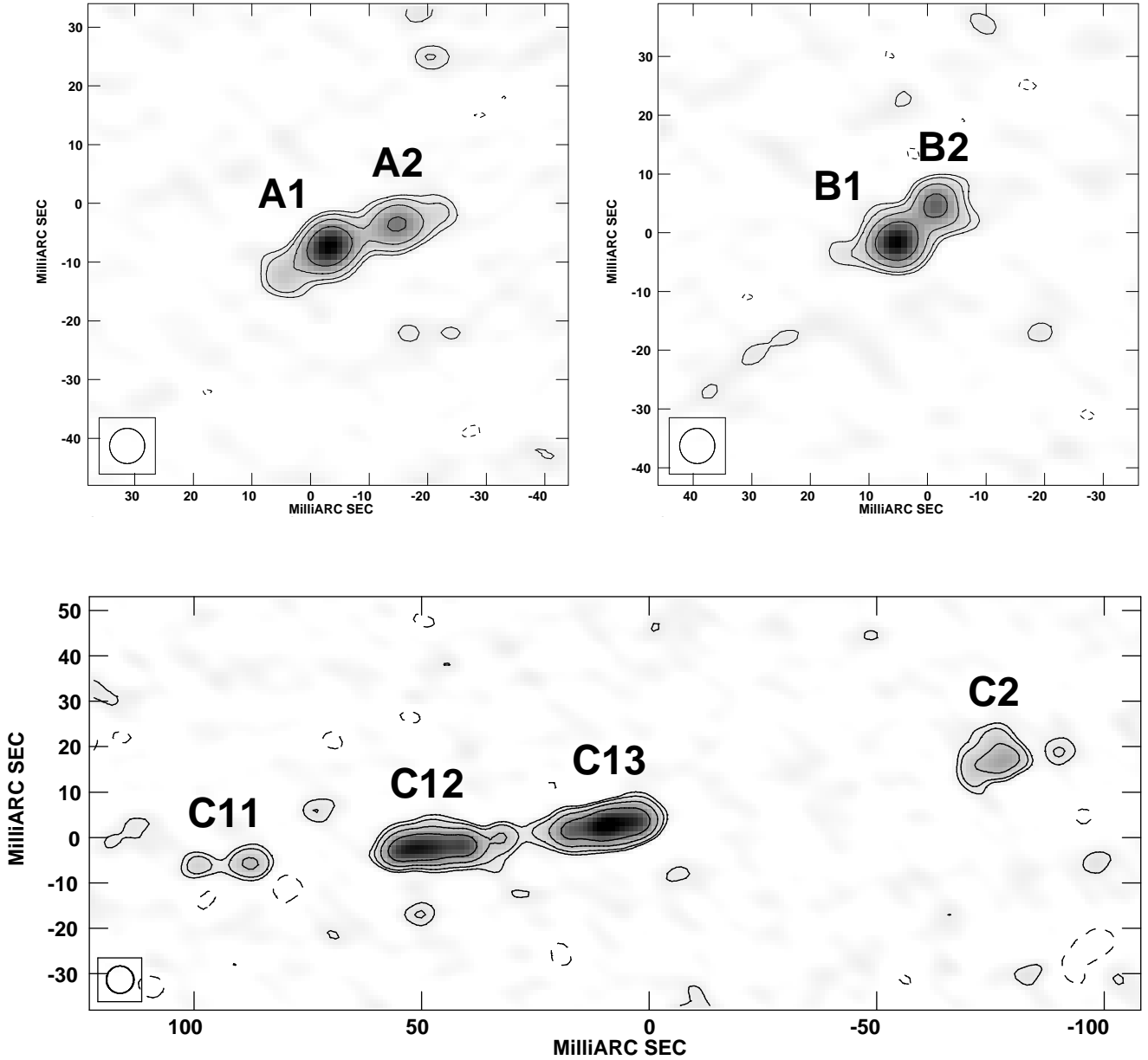


Figure 1. *European VLBI Network (EVN) 5-GHz radio images of regions A, B and C of 2016+112.* Contour levels indicate $(-3, 3, 5, 10, 20)$ times the rms noise level of $0.14 \text{ mJy beam}^{-1}$. One notices the jet-like substructure in images A and B, and the apparent ‘mirror-symmetry’ of components C_{12} and C_{13} , suggesting opposite parties due to lensing. The model proposed in this paper assumes that both components are images of a quadruply-lensed part of the source, which is associated with the counter-jet in components A_2 and B_2 , the core of the source. Components C_{11} and C_2 are presumably steep-spectrum images of intrinsically faint (but highly magnified) substructure further along the counter-jet (i.e. west of A_2 and B_2). The restoring beam has a FWHM of 6 milli-arcsec.

prevent fringe-rate and delay smearing over the 4 arcsecond field of view, the data associated with 2016+112 were maintained as 28 contiguous 2 MHz channels with a visibility averaging time of 2.5 seconds. The calibrated 2016+112 data were Fourier transformed and a naturally weighted, tapered

image of the full field was produced. All three main regions of emission A, B and C were clearly detected and the image was used as an input model for subsequent (phase-only) self-calibration. Since 2016+112 is a rather faint, resolved radio source, improvements to the original phase solutions were

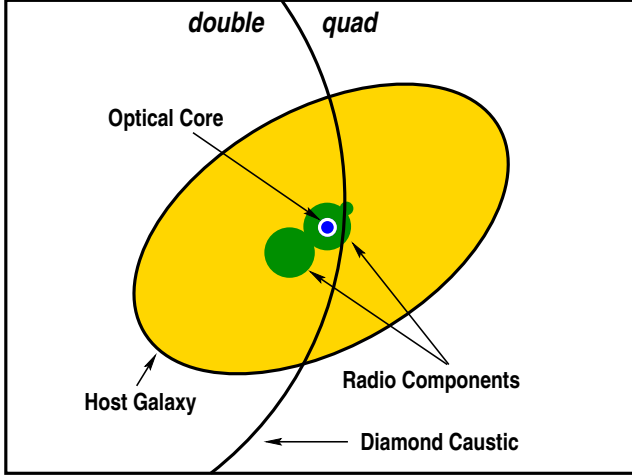


Figure 2. A schematic view of the proposed source structure for 2016+112. The AGN, associated radio core and part of host galaxy and the second radio component are doubly imaged. Part of the second radio component and the host galaxy are quadruply imaged. The components are not drawn to scale, nor do the ellipticity and position angles of host galaxy and other structures necessarily represent those of the true underlying source.

only obtained by employing a relatively long solution interval (13 minutes) over the entire frequency band (56 MHz). CLEANed maps of the three main regions of emission are presented in Fig.1. All the maps are naturally weighted (the rms noise level is $\sim 140 \mu\text{Jy beam}^{-1}$) and the FWHM of the circular restoring beam is 6 mas.

To obtain the positions and flux-densities of the radio components in regions A, B and C, elliptical Gaussians were fitted to the images. Images A and B were fitted by two Gaussians. Images C_{12} and C_{13} could not be fitted by a single elliptical Gaussian and were therefore fitted by two Gaussians (a and b , respectively). The results of these fits are listed in Table 1.

3 THE SOURCE

Based on the optical/IR and radio observations of 2016+112 (see Sections 1 and 2), we postulate the following simple picture for lensed source (see also Langston et al. 1991 and Benitez et al. 1999 for analogous models). First, we assume that optical continuum emission of images A and B is an AGN (possibly a type-II quasar) near the core of some faint underlying host galaxy, which is not detected at A and B due to its very low surface brightness compared to the AGN. Second, the EVN radio images at 1.7 GHz of A and B indicated extended structure to the NW (Heflin et al. 1991; Garrett et al. 1996). This has now been confirmed by the high-resolution EVN observations at 5 GHz presented in Sect.2, showing that both components consist of at least two subcomponents. We assume that the flatter-spectrum subcomponents seen at 5 GHz (A_2 and B_2) are associated with the optical continuum core and the other two (A_1 and B_1) are jet-features. Because the constraints from the optical emission are not used at this level of positional accuracy (few mas), this particular choice is of little relevance.

Additionally, strong spectral lines (e.g. Ly- α , C-IV, N-V, Si-IV) are seen near images A, B and C' (e.g. Schneider et al. 1986, 1987; Lawrence 1996; Yamada et al. 2001). However, the line widths are very narrow compared to a typical quasar spectrum drawn from the same redshift range (see Steidel et al. 2001). This is a puzzle, although it could be that line emission from the BLR is obscured, as suggested by Yamada et al. (2001), and that only the NLR further from the core is seen. This would also explain why the Ly- α emission is not exactly coincident with A, B and C' , but offset from C' by ~ 1 WFPC2 pixel when aligned with A and B. These narrow-line spectra are indicative of a type-II quasar (Yamada et al. 2001), which is supported by the X-ray brightness of the source (Chartas et al. 2001). A schematic picture of the source is shown in Fig.2.

Qualitatively, this source structure can explain both the optical and radio data of 2016+112 available to date, if the diamond caustic (fold) crosses the source as indicated in Fig.2: (i) the optical core is doubly imaged at A and B, because it falls outside the diamond caustic, (ii) most of the associated radio structure is also doubly imaged near A and B, (iii) only part of the radio structure, associated with the counter-jet near radio subcomponents A_2 and B_2 , is quadruply imaged, such that the apparent magnifications of the associated images C_{12} and C_{13} appear much smaller than what could be expected based on their flux-density and proximity to the critical curve, (iv) components C_{11} and C_2 are steep-spectrum emission further along the counter-jet, which are quadruply imaged but only detected near C because of the very high magnification near the critical curve, (v) part of the underlying host galaxy is doubly imaged, but is too faint to be seen at images A and B as a result of the bright AGN emission (and its associated PSF), (vi) the other part of the host galaxy is quadruply imaged, resulting in the highly magnified arc (i.e. complex C'), (vii) similarly the extended Ly- α emission (Lawrence et al. 2001), as well as the narrow-line emission in general (e.g. Yamada et al. 2001) is expected to surround the optical core and is part doubly and part quadruply imaged (i.e. that part inside the diamond caustic) and therefore seen near A, B and C' . This is supported by the idea that the emission-line ratios near C' are more consistent with it originating further from the core (Yamada et al. 2001). Although the proposed model might appear very complicated, it is precisely the complex lensed structure one expects from AGNs – which are wealthy in wavelength-dependent structure on sub-arcsec scales – if they happen to cross a caustic.

Support for the suggestion that part of the radio source crosses the caustic is given by the actual ‘merger’ of radio components C_{12} and C_{13} at the few- σ level of the surface-brightness contours in Fig.1. This *only* occurs if part of the source at that surface-brightness level actually crosses the caustic in the source plane. The critical curve crosses precisely that point in the image plane where the two images merge (i.e. the ‘saddle-point’ in the surface brightness distribution between C_{12} and C_{13}) (e.g. Kochanek, Keeton & McCleod 2000). Due to the conservations of surface brightness in gravitational lensing, we expect the point where images C_{12} and C_{13} merge to be associated with extended structure north-west of A_2 and B_2 at the few- σ contour level as well (see Fig.1). Images C_{12} and C_{13} are associated with very compact (i.e. a few μas) substructure in the

Comp.	RA (arcsec)	Dec (arcsec)	$S_{5\text{ GHz}}$ (mJy)	r_{AB}	PA ($^{\circ}$)	p_{\pm}
A ₁	+0.0000	+0.0000	8.0(0.3)	1.0(0.0)	-71.7	+
A ₂	-0.0121	+0.0040	4.5(0.3)	—	—	+
B ₁	-3.0057	-1.5040	7.3(0.3)	0.9(0.1)	-48.5	—
B ₂	-3.0126	-1.4979	4.2(0.3)	—	—	—
C ₁₁	-2.0111	-3.2331	1.9(0.3)	—	—	—
C _{12a}	-2.0455	-3.2300	3.8(0.3)	—	+95.1	—
C _{12b}	-2.0542	-3.2294	13.9(0.5)	—	+93.9	—
C _{13a}	-2.0937	-3.2241	8.7(0.4)	—	-80.2	+
C _{13b}	-2.0855	-3.2254	9.8(0.4)	—	-81.0	+
C ₂	-2.1749	-3.2101	5.6(0.5)	—	—	+

Table 1. Constraints on the model from the 5-GHz EVN data (Sect.2). Column (1): The component’s name as in Garrett et al. (1996). Columns (2-3): The positions determined from Gaussian fits to the 5-GHz EVN images. The positional error is 1 mas with respect to A₁. Column (4): The total flux-density and error on the last significant digit (within parentheses) of each of the components. Column (5): The flux-density ratios r_{AB} between the A and B components, estimated from the radio data in Garrett et al. (1996) and Sect.2. Column (6): The position angles (PA) of the presumed jet direction, measured in the direction A₁→A₂, B₁→B₂, C_{12b}→C_{12a}→C₁₁ and C_{13b}→C_{13a}→C₂ from north to east. Column (7): The parities p_{\pm} , based on general assumption of the source structure and geometry of the time-delay surface (e.g. Blandford & Narayan 1986).

counter-jet, which unfortunately is barely observable near images A and B, due to their relatively low magnifications (see Sect.5 below) and ofcourse the finite resolution of the observations. This is even stronger the case for the faint and steep-spectrum emission from C₁₁ and C₂.

In the model by Langston et al. (1991) the second flat-spectrum source component (i.e. the component associated with A₂ and B₂) lies almost fully *inside* the diamond caustic, whereas the steeper spectrum component straddles the caustic. Nair & Garrett (1997) showed, however, that this particular model predicts the inner two images of complex C to be steep spectrum and the outer two flat spectrum, opposite to observations. On this basis, the model from Langston et al. (1991) was rejected. In the model proposed here, however, the steeper spectrum component lies fully *outside* the diamond caustic, whereas only a small part of the flat-spectrum component straddles the caustic from the outside. This small part (i.e. the counter-jet) inside the caustic is quadruply imaged and highly magnified, creating images C₁₂ and C₁₃. Note that the direction or merging of images C₁₂ and C₁₃ is perpendicular to the caustic near the source position (Fig.3 below), as must generally be true for a single screen model. Further inside the caustic, we postulate that the spectrum of the counter-jet steepens and that a small subcomponent is lensed in to images C₁₁ and C₂. Both of these are only seen near C, because of their exceedingly high magnifications (Sect.5).

This type of lens-source configuration is not uncommon. Several radio gravitational lens systems have been observed with part of the source inside and part of the source outside the diamond caustic (e.g. Einstein rings). In particular, the JVAS/CLASS lens B1938+666 has a radio jet structure crossing the diamond caustic near the cusp, although in this case most of the source lies inside the caustic (King et al. 1997), whereas in 2016+112 only the counter-jet is quadruply imaged.

The question is now whether we can also *quantitatively* explain the *primary constraints* (e.g. radio and optical image positions, the jet position angles (PA) and the flux-density ratios), and whether the resulting model is in agreement with *secondary constraints*, such as the properties of the

host galaxy (D) and the detection of one or more nearby mass concentrations in weak-lensing (Clowe, Tretham & Tonry 2001) and spectroscopic studies (Soucail et al. 2001).

4 THE LENS & FIELD

First, we associate a singular isothermal elliptical (SIE) mass distribution (e.g. Kassiola & Kovner 1993; Kormann, Schneider & Bartelmann 1994; Keeton, Kochanek & Seljak 1997) with the primary lens galaxy D, although a mass model with a steeper or more shallow mass profile is not a priori excluded (e.g. Benitez et al. 1999). In light of the present uncertainties, especially about external perturbers, we feel it is not yet warranted to explore more detailed lens mass models. We associate the center of the mass distribution (MD) with the centroid of the surface brightness distribution (SBD) of galaxy D, measured from the *Hubble Space Telescope* (HST) NICMOS *F160W*-band image (CASTLES; e.g. Muñoz et al. 1998), i.e. $(-1.740 \pm 0.003, -1.782 \pm 0.003)$ arcsec with respect to image A. In general, good agreement is found between position angles of the SBD and MD of lens galaxies (Keeton, Kochanek & Seljak 1997). To avoid underconstraining the mass model, we have chosen to fix the position angle of the MD at the observed SB value of -59 ± 2 degrees (see CASTLES web page). The only free parameters of the MD of lens galaxy D are therefore the axial ratio (f) and the central velocity dispersion ($\sigma_{||}$; as defined in Kormann et al. 1994).

To model the surrounding field, we place a singular isothermal sphere (SIS) mass distribution (designated M₁) at the position (60.0, 24.0) arcsec north-west of image A, where Clowe et al. (2001; see Sect.1) find a significant weak-lensing signal. A SIS fit to the weak-lensing shear field suggests a velocity dispersion of 970^{+150}_{-180} km s⁻¹ (1- σ errors; assuming a redshift of unity). We constrain the velocity dispersion of M₁ to this value. In addition, Soucail et al. (2001) have spectroscopically confirmed the presence of an overdensity of at least six red galaxies at the redshift of lens galaxy D. They estimate a velocity dispersion of 771^{+430}_{-160} km s⁻¹. Clowe et al. (2001) do not find a strong shear signal at this position ($\sigma = 560^{+220}_{-480}$ km s⁻¹; 1- σ errors).

Defl.	RA (")	Dec (")	f	PA (°)	$\sigma_{ }$ (km s ⁻¹)
D	[-1.740]	[-1.782]	0.75–0.77	[-59]	320→342
M ₁	[+24.0]	[+60.0]	[1.0]	[0.0]	[970]
M ₂	-11.6→-2.0	0.8→-0.4	[1.0]	[0.0]	[560]→[175]

Table 2. The fixed (between brackets) and reconstructed mass-model parameters for the primary lens galaxy D and the two SIS mass distributions M₁ and M₂. The arrows indicate how the values change as the velocity dispersion of M₂ is lowered from 560 to 175 km s⁻¹. In addition to the mass distributions, an external shear (γ_{ext}) is found with strength 0.12→0.07 and position angle $-24^\circ \rightarrow -51^\circ$.

The low SNR of the observations, however, does not allow one to exclude it. We include this mass distribution to first order by modeling it as a SIS (M₂). This is done in order to test whether an additional mass distribution is indeed required by the strong-lensing constraints, as suggested by these previous authors. We allow the velocity dispersion of M₂ to vary between 560–175 km s⁻¹ and let its position be free. The upper limit is roughly defined, such that M₂ does not result in additional observable images of the background source, although this constraint could be lifted if this mass distribution has a large finite core and is not capable of multiple imaging. Similarly, the lower limit avoids additional sub-images of A, when M₂ nearly coincides with its position (see Sect.5). In the latter case, the velocity dispersion of M₂ is of galactic scale (few hundred km s⁻¹), in which case the core radius is typically small. We include an external shear with both its strength and positional angle as free parameters.

4.1 Constraints

As primary constraints on this starting model, we use the observed properties of images A, B, C₁₂ and C₁₃, as found from the HST NICMOS *F160W*-band (e.g. CASTLES) and EVN 5-GHz images (Sect.2; Table 1). The relative positions of A and B in the optical and radio agree to within the measurement errors. There appears to be a slight offset in declination between the *H*-band emission of complex C' in the HST image and the positions of the EVN radio components. It amounts, however, to only ~ 1 pixel and in light of the uncertain structure of the host galaxy, we render this difference unimportant at present. The brightness ratio between images A and B in the HST NICMOS *F160W*-band image is 1.03 ± 0.02 , whereas Garrett et al. (1996) find 0.84 ± 0.01 at 1.7 GHz. Several other radio observations indicate a ratio of ≈ 0.9 (see Nair & Garrett 1997). We adopt a value $r_{AB} = 0.90 \pm 0.10$, where the uncertainty accounts for possible variability. However, the source does not appear to vary strongly (Haarsma et al. 2001). We do not use the positions of images C₁₁ and C₂ as constraints. According to the source model (Sect.3; Fig.2), they are part of the source structure associated with lensed images A₂ and B₂. They are significantly more resolved in the EVN 5-GHz observations (Sect.2) and have steeper spectra compared with the other images between the EVN 1.7 and 5-GHz. Hence, they are probably not part of the dominant emitting region of the source that is responsible for images A₂, B₂, C_{12a/b} and C_{13a/b}. The emission from C₁₁ and C₂ could originate further along the counter-jet, which presumably has a steeper spectrum (Sect.3). We assume that the emission from C_{12a} and C_{13a} is associated with structure of the unresolved im-

ages A₂ and B₂, within a 1-mas radius from their respective centroids. Although this particular choice might seem arbitrary, it is probably conservative based on the notion that from an inverse Compton limit of $\sim 10^{12}$ K on the brightness temperature of these radio sources, a component size for A₂ and B₂ as small as ~ 0.1 mas can be expected. If the axial ratios of the components are large (i.e. jet-like), the emission region could easily ‘stretch’ to 1 mas or larger in one direction. We do *not* use the flux-density ratios between images A₂, B₂ and complex C, because the source structure lies on a caustic and consequently has a strong magnification gradient over its extent. The source can therefore not be treated as a point source, rendering the use of a flux-density ratio very difficult. All constraints are listed in Table 1.

5 RESULTS

Using the mass model and constraints discussed above, we vary the nine free parameters using the simulated annealing downhill simplex method described in Press et al. (1992), until the difference between the observed and recovered image properties are minimized in terms of the χ^2 -value (e.g. goodness-of-fit). Using different starting values of the parameters, we ensure that the final solution is close to the absolute minimum in the χ^2 -space.

We vary the velocity dispersion of M₂ between 560 and 175 km s⁻¹ (see above) and minimize χ^2 for the other free parameters. The goodness-of-fit χ^2 (for two degrees of freedom) of the best models increases only marginally between these upper and lower limits on the velocity dispersion of M₂, i.e. from 1.1 to 1.5 respectively. This indicates a strong degeneracy in the lens model, between the velocity dispersion and position of M₂ and the external shear. The velocity dispersion and axial ratio of G1 are only marginally affected. We note that the χ^2 -values can not be used to calculate a likelihood for the model, because we did not strictly use measurement errors for all constraints. The image positions, flux-ratio, PA's and parities are recovered in good agreement with the constraints (Table 1), given the uncertainties in the structure of the lensed images. The recovered image properties, inferred magnifications and time-delays are listed in Table 3. In Fig.3, we show the image configuration, critical curve, caustics and time-delay surface of this model.

In Table 2, we have listed the recovered parameters of the lens galaxy D and two additional mass structures M₁ and M₂. We find that the SD axial ratio $f = 0.75\text{--}0.76$ of galaxy D is somewhat larger than that determined from its SB distribution, i.e. 0.57 ± 0.01 , as seen in the HST NICMOS-*F160W* observations, (e.g. CASTLES web page; see also Benitez et al. 1999). The velocity dispersion of 320–340 km s⁻¹ of galaxy D implies a rest-frame mass-to-light

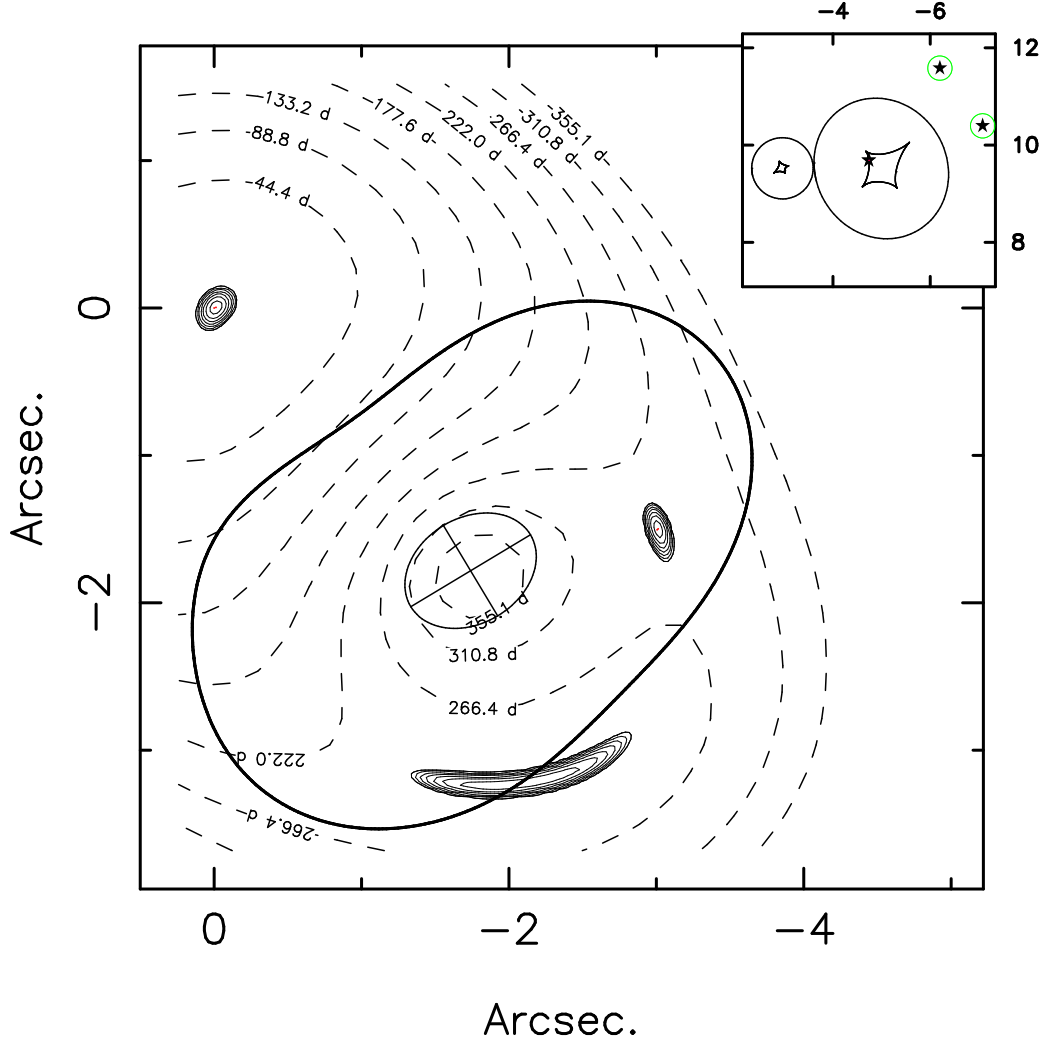


Figure 3. The model of 2016+112 as indicated in Table 2, assuming M_2 is an L_* galaxy with $\sigma_{||}=225 \text{ km s}^{-1}$ at $(-3.2'', -0.4'')$ from image A. The thick line indicates the critical curve. The ellipse indicates the position, flattening and position angle of the primary lens galaxy (i.e. D), whereas the dashed lines indicate constant time-delay contours. The subpanel (units in arcsec) shows the caustics of galaxies D and M_2 , the source (indicated by the star inside the caustics) and the two Ly- α patches (stars with circles; see Sect.6). The caustics are displaced to the north from the primary lens galaxy by ~ 10 arcsec due to a massive structure M_1 , inferred from weak lensing (see text).

ratio of $(M/L)_H \approx 1.7 \cdot h_{65} M_\odot / L_{H,\odot}$ (no evolutionary correction), assuming a singular isothermal sphere to calculate the mass inside the Einstein radius, an H-band magnitude for lens galaxy D of 18.12 ± 0.04 (see CASTLES web-page) and the galaxy models from Poggianti (1997). This mass-to-light ratio compares well with those found for other lens galaxies (e.g. Jackson et al. 1998), which indicates that the image separation should not be significantly affected by a mass contribution with a different mass-to-light ratio (e.g. a dark cluster). In that case, the lens galaxy would most likely not have been on the Fundamental Plane of early-type galaxies either (Kochanek et al. 2000).

The model also indicates the presence of an external shear with a strength γ between 0.07 and 0.12 and a position angle between -24 and -51 degrees, depending on the velocity dispersion of M_2 . If we investigate the I-band image (Fig.2 in Soucail et al. 2001) in more detail, there ap-

pears to be a ‘filamentary structure’ of high-redshift galaxies running across the lens system. This ‘filament’ is *not* dynamically related, because it contains galaxies over a very different range of redshifts ($z \approx 0.6-1.1$), but it might be responsible for the shear at the position of 2016+112. On the other hand, the closeness of the position angle of the external shear and that of the SB of galaxy D, for low velocity dispersions of M_2 , might also indicate that either the mass distribution of galaxy D has a different radial mass profile or that its flattening is a function of radius.

Finally, we note the remarkably high magnification ($\mu \sim 300$) of images C_{12} and C_{13} , although the precise value is sensitive to the details of the model input (see also below). This is the highest (inferred) magnification for any known lens system. Because it is primarily directed tangentially and the jet direction is nearly perpendicular to the fold caustic, according to the model, any relativistic motion

Comp.	RA (arcsec)	Dec (arcsec)	$r_{\{B,C\}/A}$	μ	$\Delta t/h_{65}$ (days)
A ₁	+0.0008/0.0008	−0.0002/0.0000	[1.0]	+4.0/3.3	≡0.0
A ₂	−0.0121/0.0121	+0.0040/0.0040	[1.0]	+4.0/3.3	3.3/9.1
B ₁	−3.0060/3.0060	−1.5036/1.5033	0.91/0.85	−3.6/2.8	255.3/291.6
B ₂	−3.0126/3.0127	−1.4979/1.4981	0.90/0.84	−3.6/2.8	254.9/286.4
C _{12b}	−2.0542/2.0542	−3.2294/3.2292	91.8/77.4	−367/252	224.1/254.6
C _{13b}	−2.0855/2.0855	−3.2254/3.2257	92.5/78.2	+369/255	224.1/254.6

Table 3. Recovered image parameters (see Table 1). The flux ratios and magnifications (assuming point-source structures) are given by $r_{\{B,C\}/A}$ and μ , respectively, and the time-delays are given by Δt with respect to the leading image A₁ (assuming the cosmological model mentioned in Sect.1). The first and second values indicate those for $\sigma_{M1}=560$ and 175 km s^{-1} , respectively. The recovered source positions for {A₁, B₁} and {A₂, B₂, C_{12b}, C_{13b}} are (1.214/5.010'', 10.143/9.670'') and (1.220/5.003'', 10.144/9.669''), respectively.

in the radio jet structure will be enhanced by a factor $\sim\mu$. Superluminal velocities of say $\sim 3h^{-1}c$ (e.g. Vermeulen & Cohen 1994) could therefore lead to *hyperluminal* velocities of $\sim 10^3 h^{-1}c$. Similarly, one can probe structure with a few micro-arcsecond intrinsic scales when observed with VLBI. On the other hand, if the lensed structure is part of the counter-jet (see Sect.3), such high velocities are no longer expected. The absence of strong variability in the source (Haarsma et al. 2001) and its GPS-type radio spectrum are also indicative of the absence of strongly relativistic motion.

One problem that we have not yet addressed is the considerable difference in angular distance between the pair components C₁₁–C₁₂ and C₁₃–C₂, which we did not include in the lens model. Given the high magnification and symmetry around the critical curve, one would expect these distances to be similar. The fact that they are not seems to argue against our model and in favor of a two lens model (Nair & Garrett 1997). However, magnifications and the magnification matrix are a function of differences in higher-order derivatives of the local lens potential (see Schneider et al. 1992). Especially in regions of very high magnification, many of these derivatives are very close to zero, because in those cases the lensed images form at very shallow extrema of the time-delay surface. It is therefore not inconceivable that even a minuscule perturbation of the local lens potential (e.g. by a globular cluster, halo substructure, etc) will have an enormous effect on the local magnification matrix, i.e. on the image magnifications and the image positions. These discrepancies near critical curves have been seen in other lens systems with very high image magnifications (Mao & Schneider 1998) and might not be uncommon in general. As an example, if we include a typical globular cluster with a velocity dispersion $\sigma=7 \text{ km s}^{-1}$ (Einstein radius of $\lesssim 1 \text{ mas}$) about 5 mas away from image C₂, it changes the magnifications of C₂ and C₁₁ considerably, but also projects them on the same position in the source plane. The magnification ratio between C₁₂ and C₁₃ remains equal to unity within a few percent. The probability of such minor perturbations is considerable, especially because one expects hundreds if not thousands of globular clusters, dwarf satellites, etc. around these massive elliptical galaxies. At higher redshift, according to cosmological CDM models, the amount of halo substructure could be even more prevalent. We are therefore not too worried about this apparent discrepancy, but are warned that even though the magnifications in complex C are very high, their precise values are quite uncertain and should only be taken as indicative.

6 DISCUSSION & CONCLUSION

We have shown that 2016+112 can be explained by a *single-screen* mass model. The observational constraints are reasonably well reproduced by the proposed model. The axial ratio of the surface MD of the lens galaxy D is somewhat larger than the axial ratio of its SB distribution, as determined from HST NICMOS *F160W*-band observations. Also its mass-to-light ratio is in good agreement with that of other lens galaxies. Surprisingly, our model is consistent with the presence of a massive mass component about 1' north-west of the lens galaxy, suggested from a weak-lensing analysis of the field (Clowe et al. 2001). We find evidence for an external shear that might result from a 'filamentary structure' of high-redshift galaxies running across the lens system roughly from east to west (see Soucail et al. 2001). This filament is not a dynamically related structure, because it contains galaxies over a wide range of redshifts. The massive dark cluster previously suggested can not be confirmed or excluded, based on the strong-lensing constraints. In particular, a single $\sim L_*$ galaxy several arcsec east of galaxy D (see Fig.3) could also be consistent with the strong lensing constraints. A faint object at that approximate position does appear on a deep R-band image, i.e. Fig.4 in Clowe et al. (2001), although we do not know whether that object is indeed a galaxy. Given the high redshift of the source, a perturbing galaxy at that position could have a wide range of redshifts (0.5–1.5), not necessarily being that of the primary lens galaxy.

Because we can explain the available data on 2016+112 with a single-screen model, we conclude that a second screen is probably no longer necessary and that the optical/IR object C' is in fact a highly magnified arc of the AGN host galaxy at $z=3.273$. Thus, we predict that optical spectroscopy of complex C' will not yield a redshift in between that of lens galaxy D and the source as previously suspected, but will instead *only* show features at the source redshift.

Our model predicts a very high magnification ($\mu\sim 300$) of images C₁₂ and C₁₃. This can be expected based on the proximity of these images (only $\sim 20 \text{ mas}$) to the critical curve passing in between them (see Fig.1). Because, the magnification is inverse proportional to the separation between the two images (e.g. Schneider et al. 1992, Chapt.6), the small separation ($\sim 40 \text{ mas}$) between the images results in an order of magnitude higher magnification than normally observed. This is enhanced by the small angle between the line joining the images and the caustic, resulting in an even smaller distance of the images to the caustic (i.e. a higher

magnification). A magnification that is 1–2 orders of magnitude larger than normally seen for two merging images ($\mu \sim 10$), can therefore be expected. This magnification could lead to observable *hyperluminal* motion with velocities of order $\sim 10^3 h^{-1} c$ of micro-arcsec-scale structure in the lensed jet, although the GPS-type radio spectrum and low variability of the source at present do not support the notion of high apparent velocities in the radio jet, especially also because our model suggests that it is the counter-jet that is being magnified.

Our source model appears to be that of a type-II quasar (e.g. Yamada et al. 2001; Chartas et al. 2001). At radio wavelengths, only the counter-jet of the source is quadruply imaged, whereas the AGN core and radio jet are doubly imaged. The host galaxy and the extended narrow-line emission around the core is part doubly and part quadruply imaged, which explains its offset from the optical and radio structures and also the difference in line ratios between images A & B and complex C (Yamada et al. 2001). The absence of BLR emission and the presence of X-ray emission (Chartas et al. 2001) further support the identification of this source as a type-II quasar.

Finally, we suggest that the two patches of Ly- α emission found by Schneider et al. (1986, 1987) could be cold gas clouds in the IGM – possibly around some nearby galaxies – that are illuminated by the emission cone coming from the AGN along the jet axes. There are indeed several objects at the positions of these patches (Soucail et al. 2001; Clowe et al. 2001), of which the brightest has the same redshift as the source (Soucail et al. 2001). When projecting the two patches on the source plane (Fig.3), using the mass model presented in this paper, we find that one lies close to the (counter) jet axis in the source plane, i.e. $\sim 20^\circ$, whereas the second patch makes an angle of $\sim 50^\circ$. Their distances to the AGN in the source plane are 1.9 and 1.5 arcsec, respectively. They are therefore not multiply imaged. If the jet is pointed towards (or away from) the observer, the real angles between the patch, AGN and observer could be smaller. The low expected metallicity for such IGM clouds could explain the strong presence of Ly- α emission lines and the absence of strong metal lines, such as the CIV lines seen near images A, B and C' (Schneider et al. 1987; Lawrence 1996). If these patches are indeed illuminated by the AGN, we expect this Ly- α emission to be highly polarized. Polarimetry observations on a 10-m class telescope could confirm this.

The ultimate test between the different one and two-lens models will be the measurement of the redshift of complex C', which can only be $z \approx 3.273$, according to model proposed in this paper.

ACKNOWLEDGMENTS

LVEK and RDB would like to thank Ian Browne for invaluable help during the initial phases of this research. LVEK also thanks Ian Browne and Sunita Nair for useful comments on a draft of the paper. The authors thank George Chartas for sending a version of their paper on *Chandra* X-ray observations of 2016+112 prior to publication. This research has been supported by NSF AST-9900866 and STScI GO-06543.03-95A.

REFERENCES

- Benítez, N., Broadhurst, T., Rosati, P., Courbin, F., Squires, G., Lidman, C. & Magain, P. 1999, *ApJ* 527, 31
 Blandford, R. & Narayan, R. 1986, *ApJ* 310, 568
 Chartas, G., Bautz, M., Garmire, G., Jones, C., & Schneider, D. P. 2001, *ApJL* 550, L163
 Clowe, D., Trentham, N., & Tonry, J. 2001, *A&A* 369, 16
 Garrett, M. A., Muxlow, T. W. B., Patnaik, A. R. & Walsh, D. 1994, *MNRAS* 269, 902
 Garrett, M. A., Porcas, R. W., Nair, S. & Patnaik, A. R. 1996, *MNRAS* 279, L7
 Haarsma, D. B., Hoekema, K. J., Hewitt, J. N., & Langston, G. I. 2001, American Astronomical Society Meeting, 198, 3703
 Hattori, M. et al. 1997, *Nature* 388, 146
 Heflin, M. B., Gorenstein, M. V., Lawrence, C. R., & Burke, B. F. 1991, *ApJ* 378, 519
 Jackson, N., Helbig, P., Browne, I., Fassnacht, C. D., Koopmans, L., Marlow, D., & Wilkinson, P. N. 1998, *A&A* 334, L33
 Kassiola, A. & Kovner, I. 1993, *ApJ* 417, 450
 Keeton, C. R., Kochanek, C. S. & Seljak, U. 1997, *ApJ* 482, 604
 King, L. J., Browne, I. W. A., Muxlow, T. W. B., Narasimha, D., Patnaik, A. R., Porcas, R. W., & Wilkinson, P. N. 1997, *MNRAS* 289, 450
 Kochanek, C. S. et al. 2000, *ApJ* 543, 131
 Kochanek, C. S., Keeton, C. R., & McLeod, B. A. 2001, *ApJ* 547, 50
 Kormann, R., Schneider, P. & Bartelmann, M. 1994, *A&A* 284, 285
 Langston, G., Fischer, J. & Aspin, C. 1991, *AJ* 102, 1253
 Lawrence, C. R., Schneider, D. P., Schmidt, M., Bennett, C. L., Hewitt, J. N., Burke, B. F., Turner, E. L. & Gunn, J. E. 1984, *Science*, 223, 46
 Lawrence, C. R., Neugebauer, G. & Matthews, K. 1993, *AJ* 105, 17
 Lawrence, C. R. 1996, *IAU Symp.* 173: Astrophysical Applications of Gravitational Lensing, 173, 299
 Lawrence, C. R. et al. 2001, in preparation
 Mao, S. & Schneider, P. 1998, *MNRAS* 295, 587
 Muñoz, J. A., Falco, E. E., Kochanek, C. S., Lehár, J., McLeod, B. A., Impey, C. D., Rix, H. -. & Peng, C. Y. 1998, *Ap&SS* 263, 51
 Nair, S. 1993, *Bulletin of the Astronomical Society of India*, 21, 425
 Nair, S. & Garrett, M. A. 1997, *MNRAS* 284, 58
 Narasimha, D., Subramanian, K. & Chitre, S. M. 1987, *ApJ* 315, 434
 Press, W. H., Teukolsky, S. A., Vetterling, W. T. & Flannery, B. P. 1992, Cambridge: University Press
 Schneider, D. P., Lawrence, C. R., Schmidt, M., Gunn, J. E., Turner, E. L., Burke, B. F. & Dhawan, V. 1985, *ApJ* 294, 66
 Schneider, D. P., Gunn, J. E., Turner, E. L., Lawrence, C. R., Hewitt, J. N., Schmidt, M. & Burke, B. F. 1986, *AJ* 91, 991
 Schneider, D. P., Gunn, J. E., Turner, E. L., Lawrence, C. R., Schmidt, M. & Burke, B. F. 1987, *AJ* 94, 12
 Schneider, P., Ehlers, J. & Falco, E. E. 1992, *Gravitational Lenses*, XIV, 560 pp. 112 figs.. Springer-Verlag Berlin Heidelberg New York
 Soucail, G., Kneib, J. -P., Jaunsen, A. O., Hjorth, J., Hattori, M., & Yamada, T. 2001, *A&A* 367, 741
 Vermeulen, R. C. & Cohen, M. H. 1994, *ApJ* 430, 467
 Yamada, T., Yamazaki, S., Hattori, M., Soucail, G., & Kneib, J. -P. 2001, *A&A* 367, 51